# Supplementary materials for the article Multivariate bias adjustment of high-dimensional climate simulations: The "Rank Resampling for Distributions and Dependence" ($R^2D^2$) Bias Correction

Mathieu Vrac

Laboratoire des Sciences du Climat et de l'Environnement (LSCE-IPSL, CNRS)
Centre d'Etudes de Saclay, Orme des Merisiers, 91190 Gif-sur-Yvette, France

*Correspondence to:* Mathieu Vrac (mathieu.vrac@lsce.ipsl.fr)

**Table 1.** Values of $S_{corr}$, corresponding to the sum of the absolute values of the elements of the difference correlations matrices for each dataset and for the different types of correlations (see text for details) in summer. Values have to be multiplied by $10^4$. Some methods and applications provide different $S_{corr}$ values depending on the reference dimension. For those cases, the mean $S_{corr}$ value is indicated and the standard deviation is indicated between brackets. Values in bold font indicate the smallest values for the line.

| | ERA-I | 1d-BC | 2d-$R^2D^2$ | 1506d-$R^2D^2$ (T2 or PR) | 3012d-$R^2D^2$ |
|---|---|---|---|---|---|
| Spearman (T) | 14.8 | 14.8 | 81.7 (+/- 94.6) | **4.5** | **4.5** |
| Pearson (T) | 14.2 | 13.8 | 81.7 (+/- 96) | **3.9** | **3.9** |
| Spearman (PR) | 58.4 | 38.9 | 71.3 (+/- 45.8) | **7** | **7** |
| Pearson (PR) | 68 | 43.9 | 68.5 (+/- 34.8) | **12.8** | **12.8** |
| Spearman (T2 vs. PR) | 46.2 | 50.7 | 17.8 (+/- 1.2) | 48.7 (+/- 5.6) | **12.6** |
| Pearson (T2 vs. PR) | 43.9 | 46.2 | 11 (+/- 2.1) | 42 (+/- 3.2) | **5.6** |
| Spearman (T and PR) | 165.6 | 155.1 | 188.6 (+/- 46.4) | 109 (+/- 11.3) | **36.8** |
| Pearson (T and PR) | 170 | 150 | 172.1 (+/- 65.3) | 100.8 (+/- 6.4) | **28** |

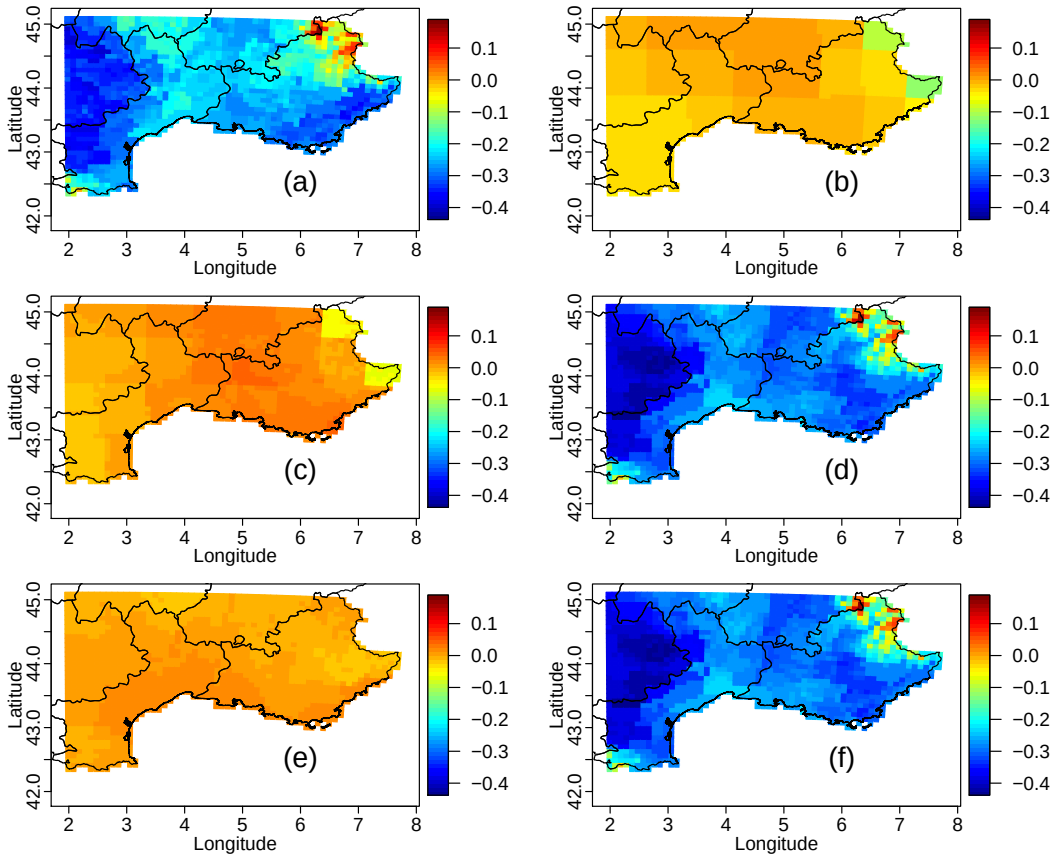


**Figure 1.** Inter-variable Spearman correlation maps in summer over the evaluation period from: (a) SAFRAN; (b) ERA-I; (c) 1d-BC (CDF-t); (d) 2d-$R^2D^2$; (e) 1506d-$R^2D^2$ on temperature and 1506d-$R^2D^2$ on precipitation; (f) 3012d-$R^2D^2$.

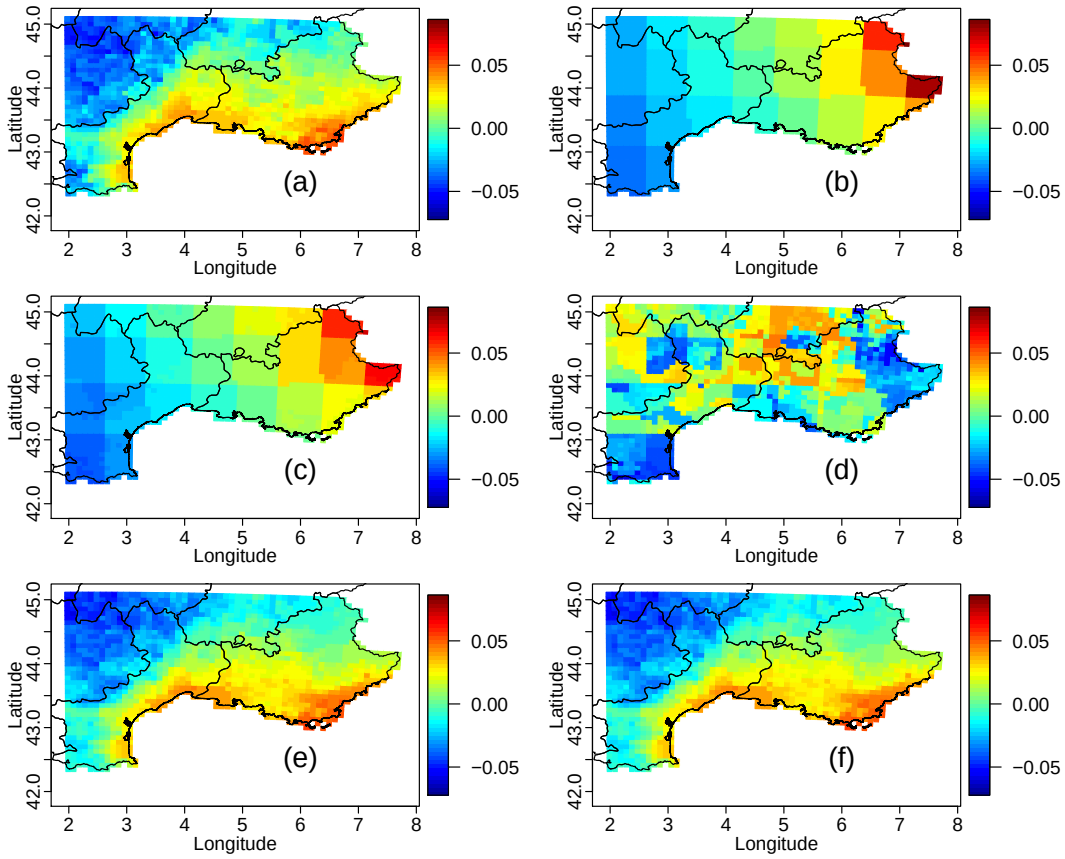


**Figure 2.** Maps of first temperature EOFs in summer over the evaluation period for (a) SAFRAN; (b) ERA-I; (c) 1d-BC (CDF-t); (d) 2d-$R^2D^2$ (with PR as reference dimension); (e) 1506d-$R^2D^2$ (on T2 only); (f) 3012d-$R^2D^2$.

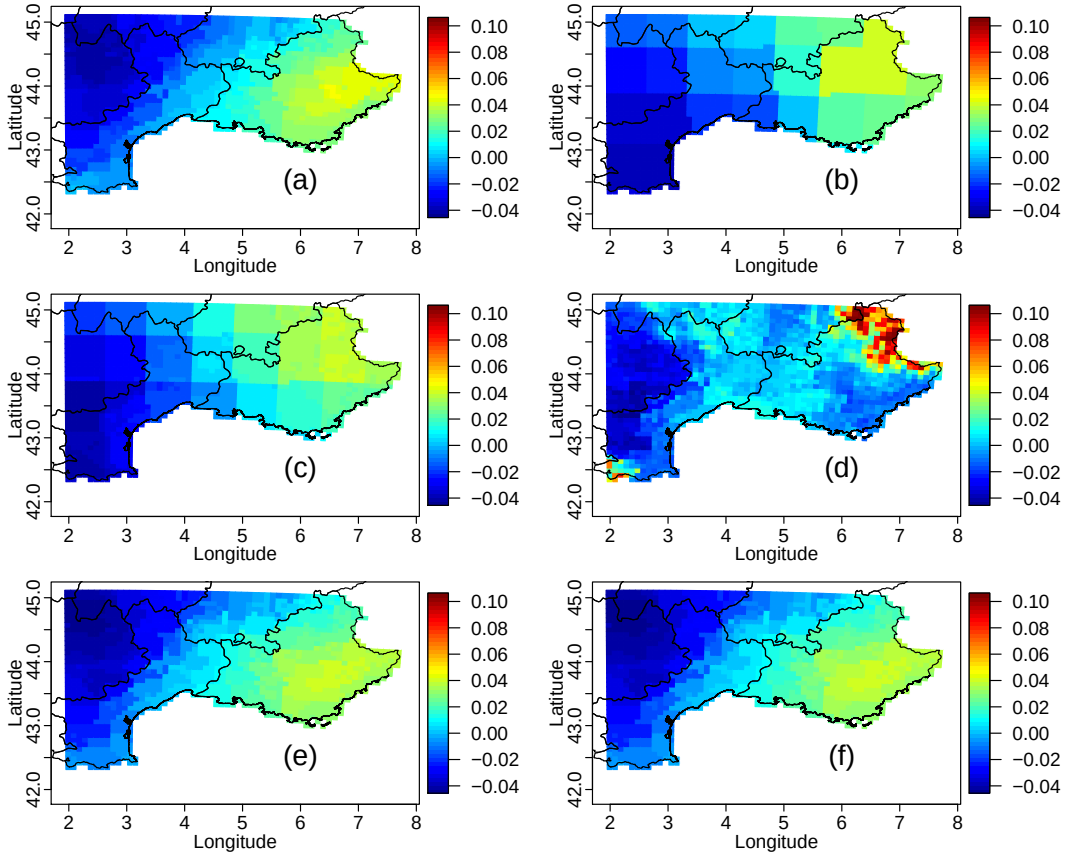


**Figure 3.** Same as Fig. 2 but for precipitation.

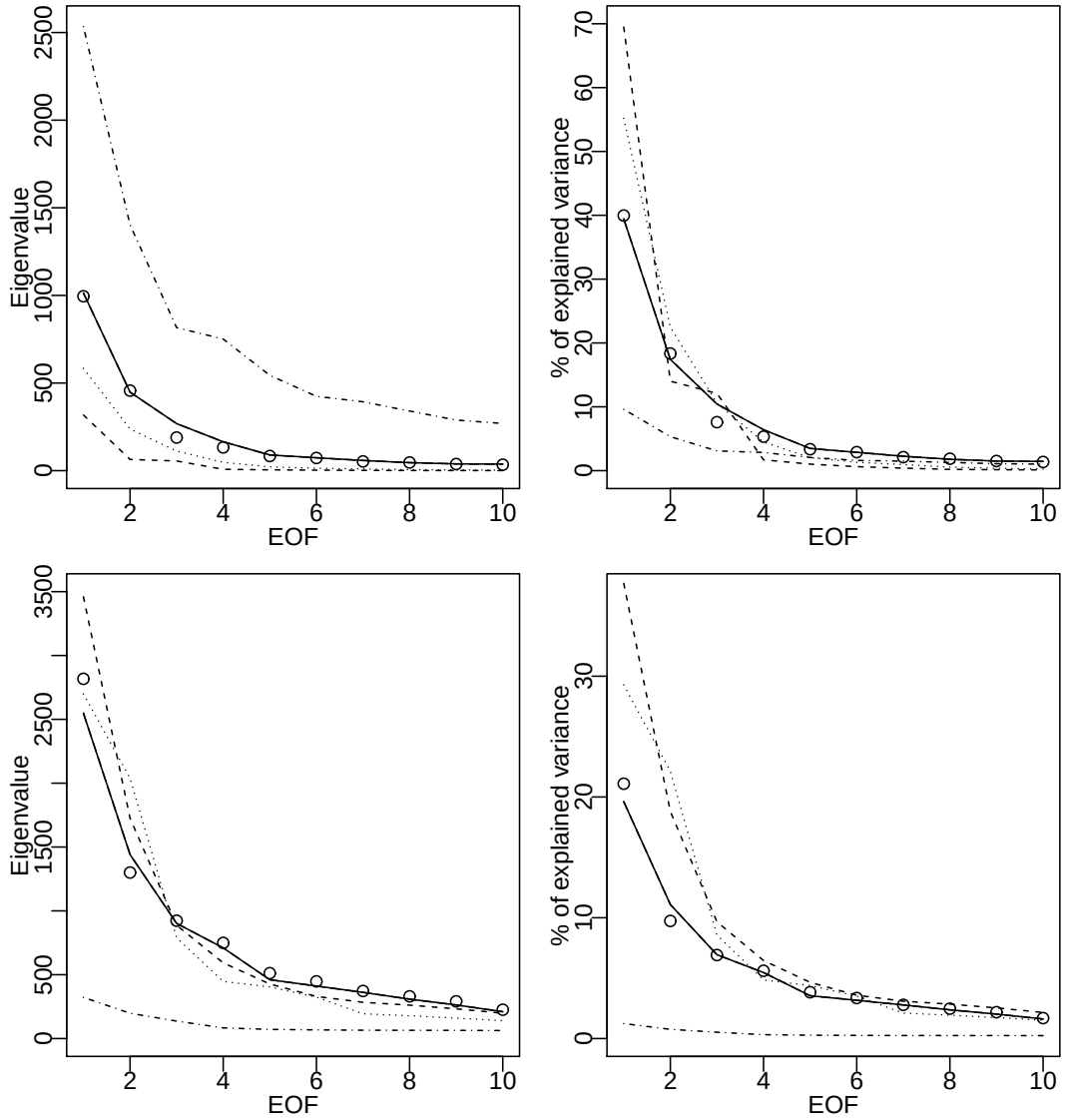


**Figure 4.** Eigenvalues (left) and percentage of explained variance (right) of temperature at 2m (first row) and precipitation (second row) in summer over the evaluation period for: SAFRAN (circles); ERAI (dashed); 1d-BC by CDF-t (dotted); 2d-$R^2D^2$ (dashed-dotted); 1506d-$R^2D^2$ (T2 or PR, long dashed); 3012d-$R^2D^2$ (solid line). Note that results of the 1506d- (long dashed) and 3012d-$R^2D^2$ (solid line) versions are the same and are therefore superimposed.

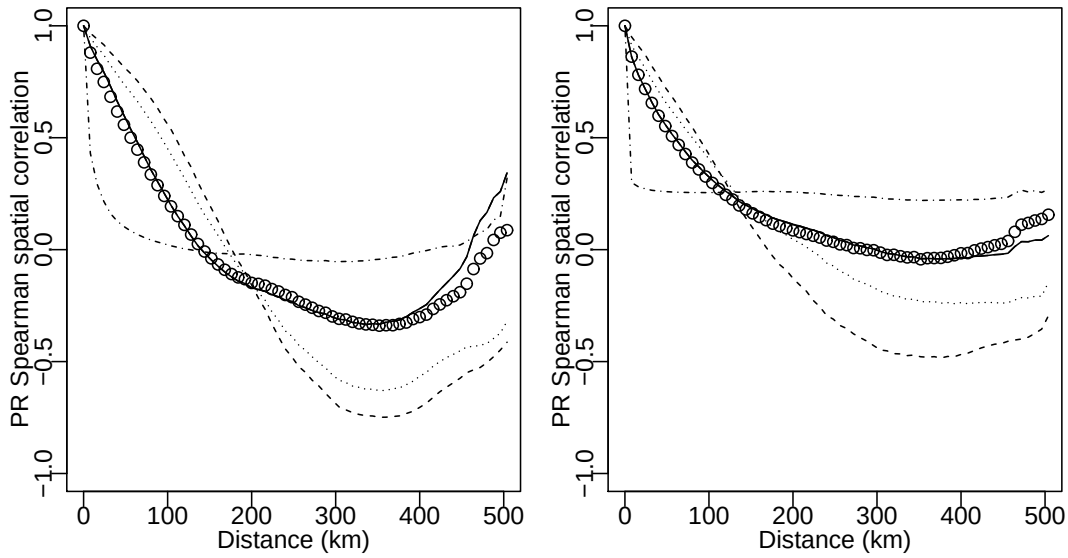


**Figure 5.** Correlograms in summer over the evaluation period for (left) temperature at 2m; (right) precipitation, from reference data (circles); ERAI (dashed); 1d-BC (dotted); 2d-BC (dashed-dotted); 1506d-BC (T2 or PR, long dashed); 3012d-BC (solid line). Note that results of the 1506d- (long dashed) and 3012d-$R^2D^2$ (solid line) versions are the same and are therefore superimposed.

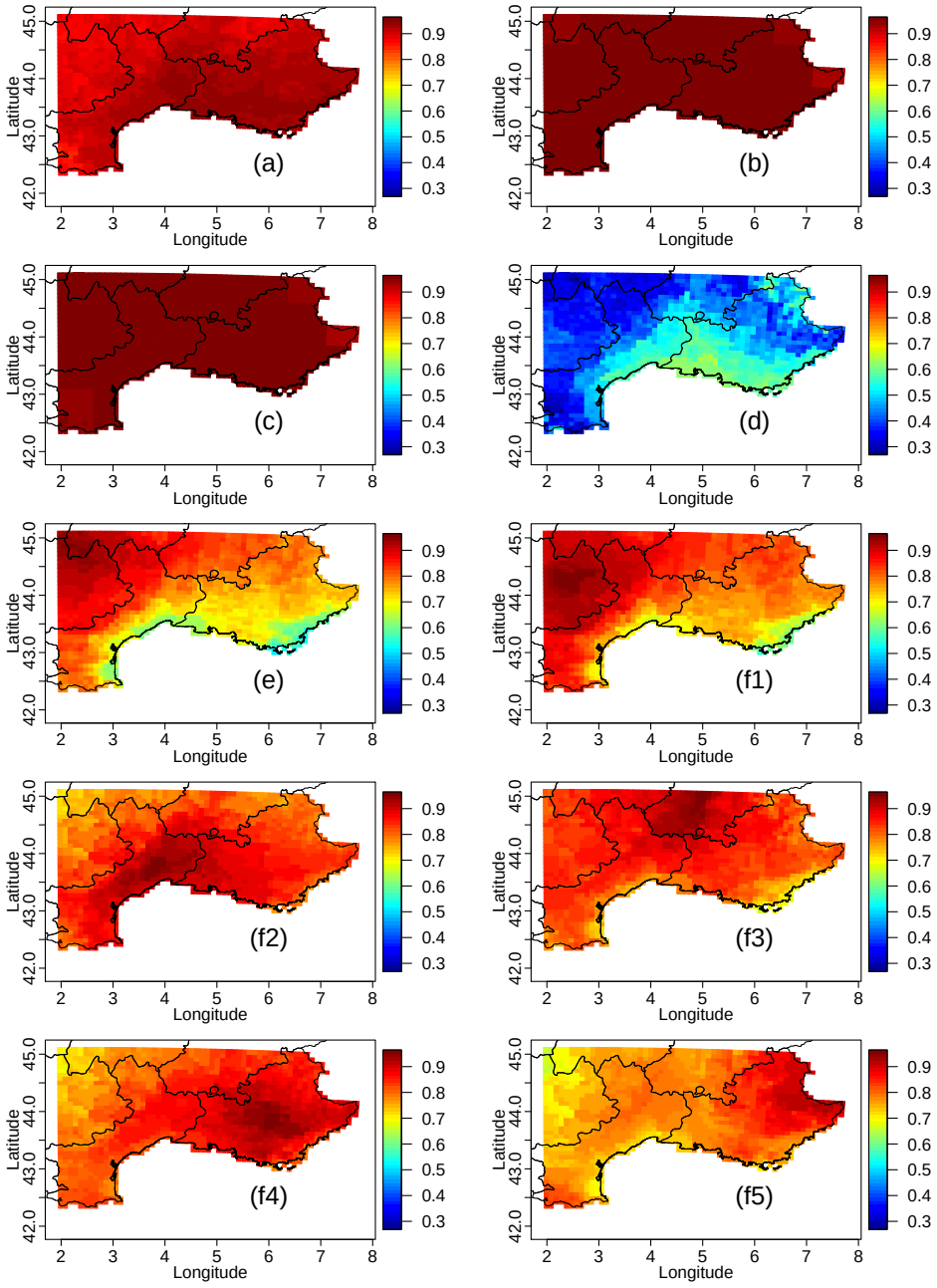


**Figure 6.** Maps of lag-1 day temperature auto-correlations in summer over the evaluation period for (a) SAFRAN; (b) ERA-I; (c) 1d-BC; (d) 2d-$R^2D^2$ (with PR as ref.dim. for each grid-cell); (e) 1506d-$R^2D^2$; (f1-5) 3012d-$R^2D^2$ with 5 different reference temperature locations.

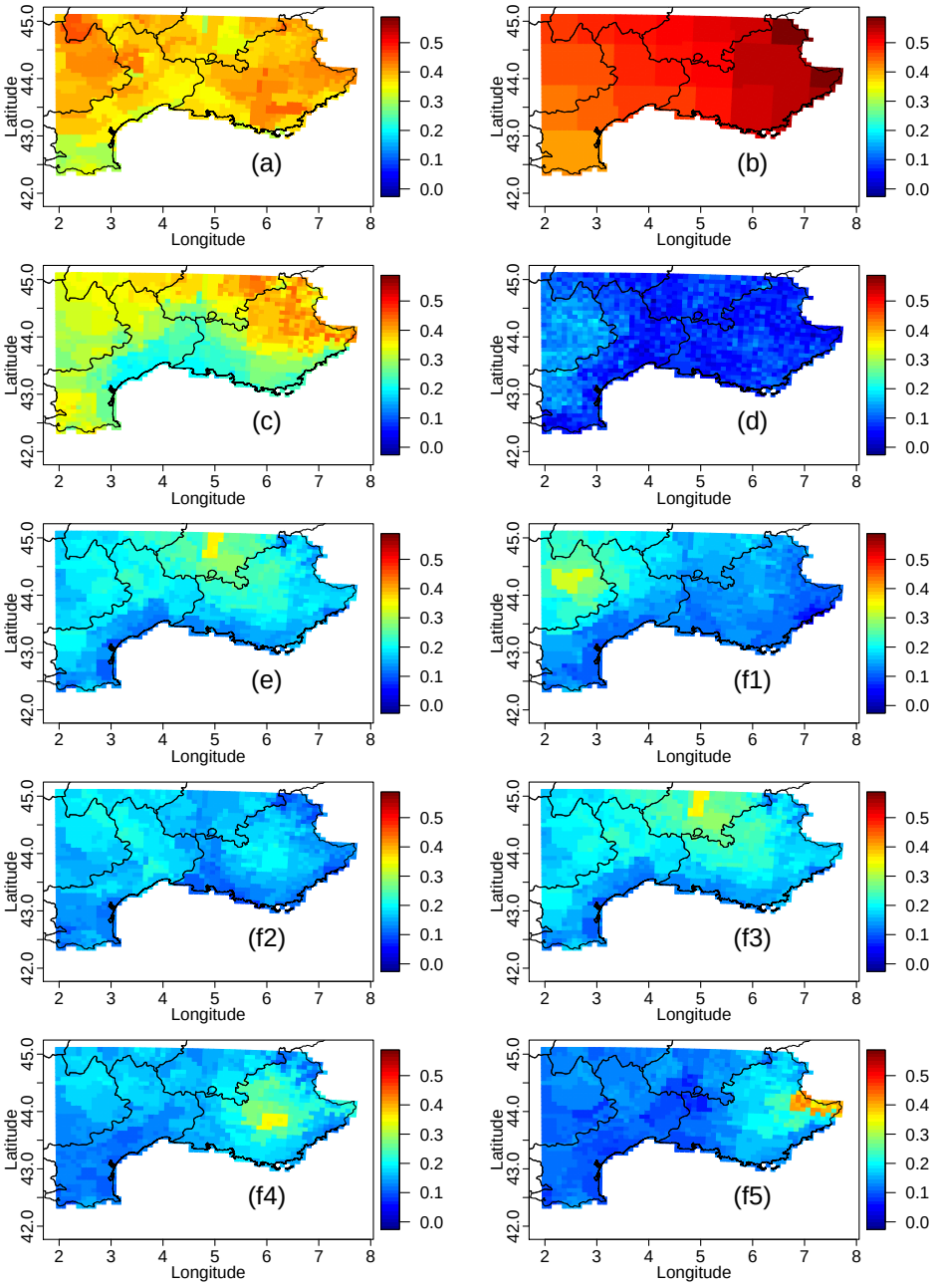


**Figure 7.** Same as Fig. 6 but for precipitation.

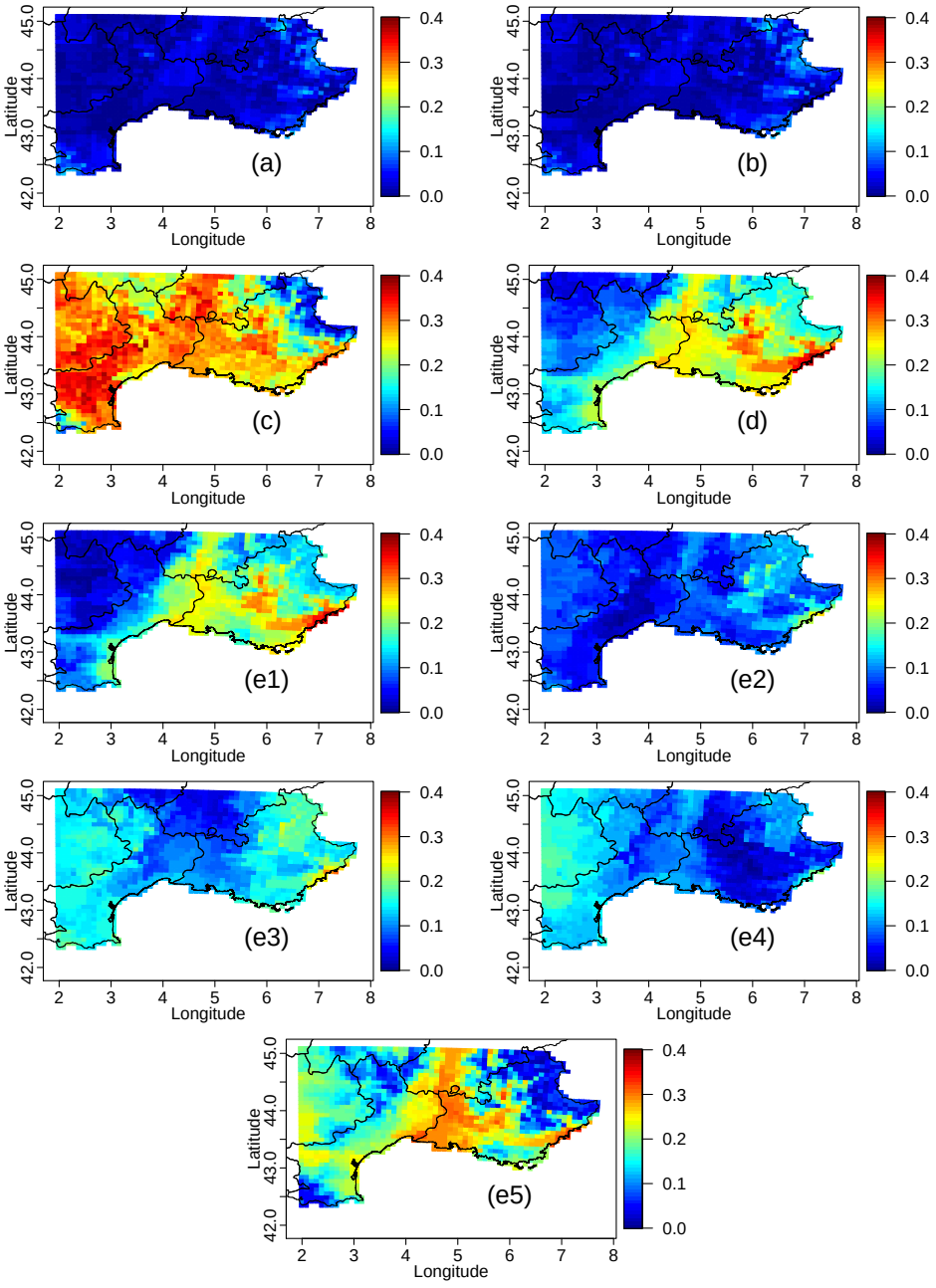


**Figure 8.** Maps of 2m-temperature MAE values (with respect to the observations in the evaluation period) calculated on lag-1 to lag-7 day Pearson correlations in winter for: (a) ERAI; (b) 1d-BC; (c) 2d-$R^2D^2$; (d) 1506d-$R^2D^2$ of T2 (example for one reference variable); (e1-e5) 3012d-$R^2D^2$ with 5 different reference temperature locations.

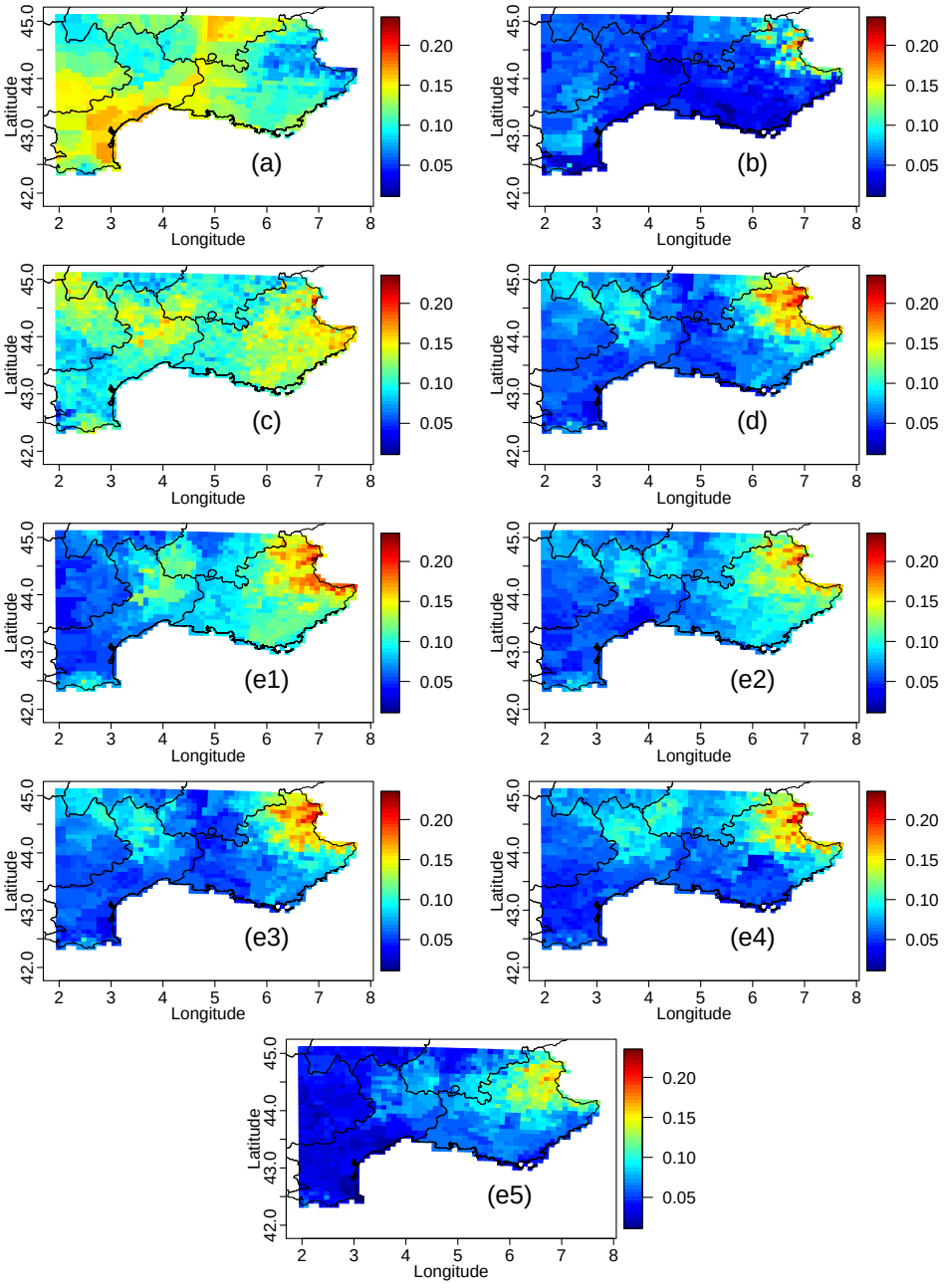


**Figure 9.** Same as Fig. 8 but for precipitation in winter.

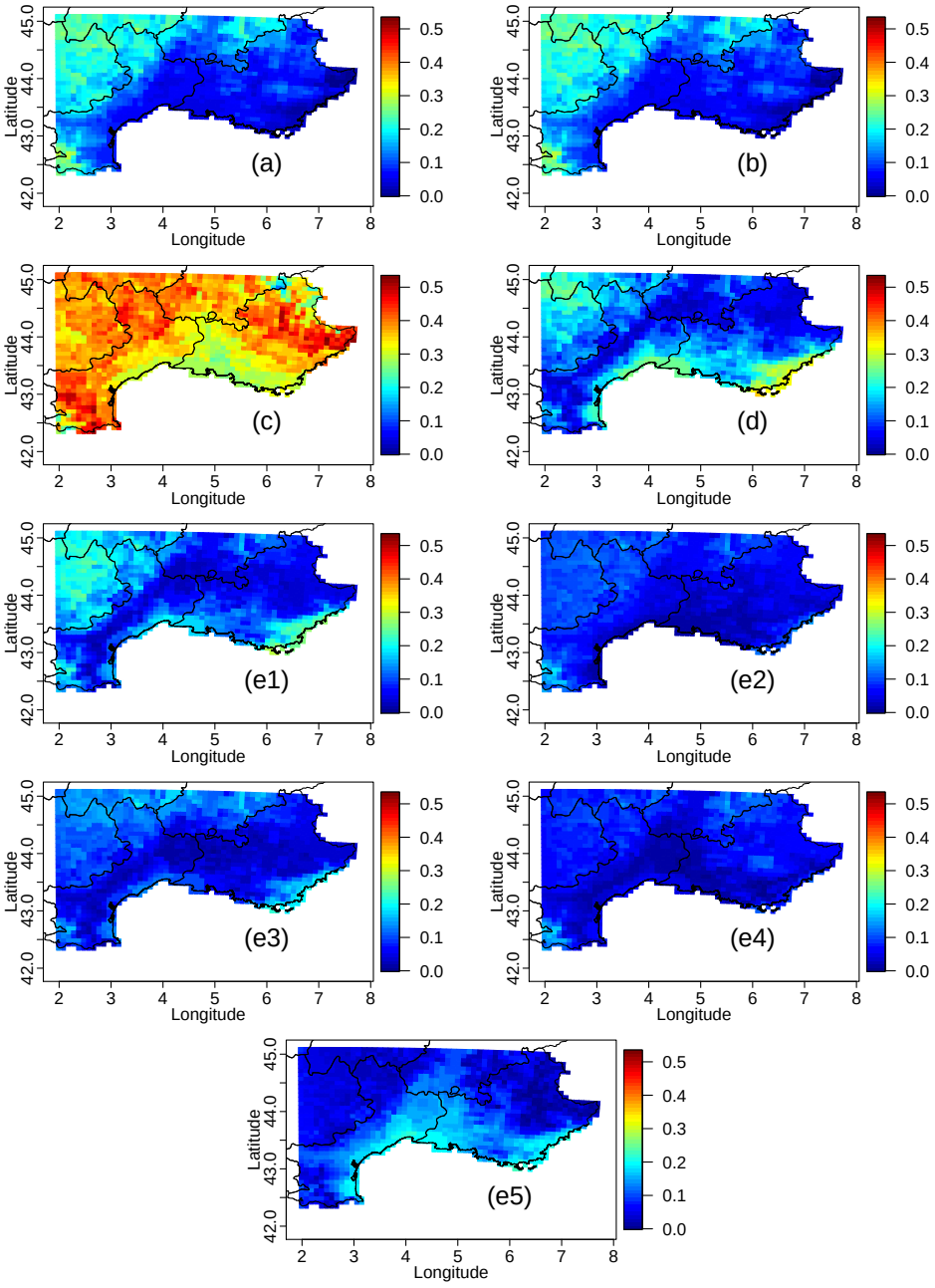


**Figure 10.** Same as Fig. 8 but for temperature in summer.

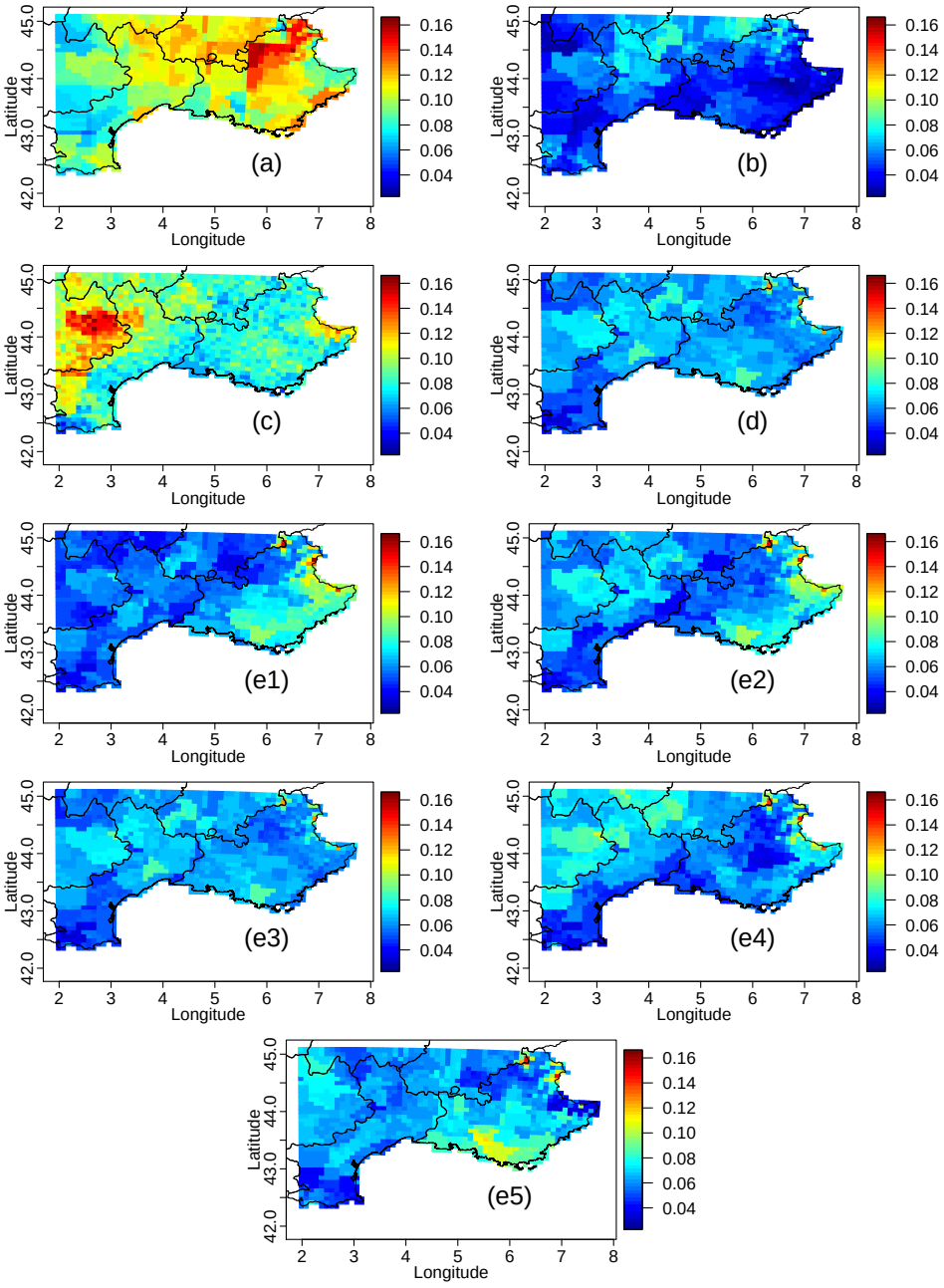


**Figure 11.** Same as Fig. 8 but for precipitation in summer.

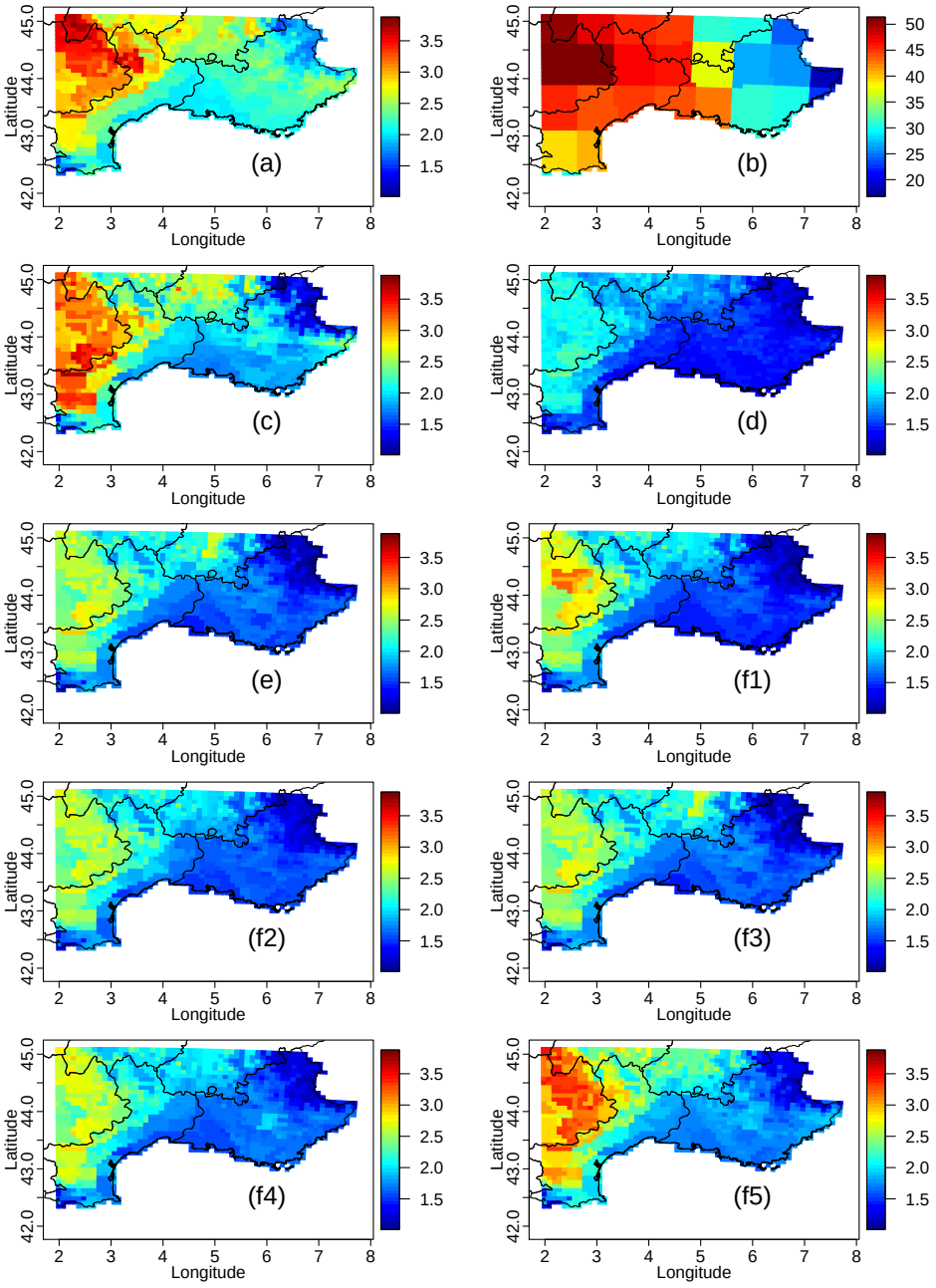


**Figure 12.** Maps of the mean wet spell lengths in winter for (a) SAFRAN; (b) ERAI; (c) 1d-BC; (d) 2d-$R^2D^2$; (e) 1506d-$R^2D^2$ (PR); (f1-5) 3012d-$R^2D^2$ with 5 different reference temperature locations. Note that the ERA-I sub-figure (b) has a range different from the others for visualization purposes.

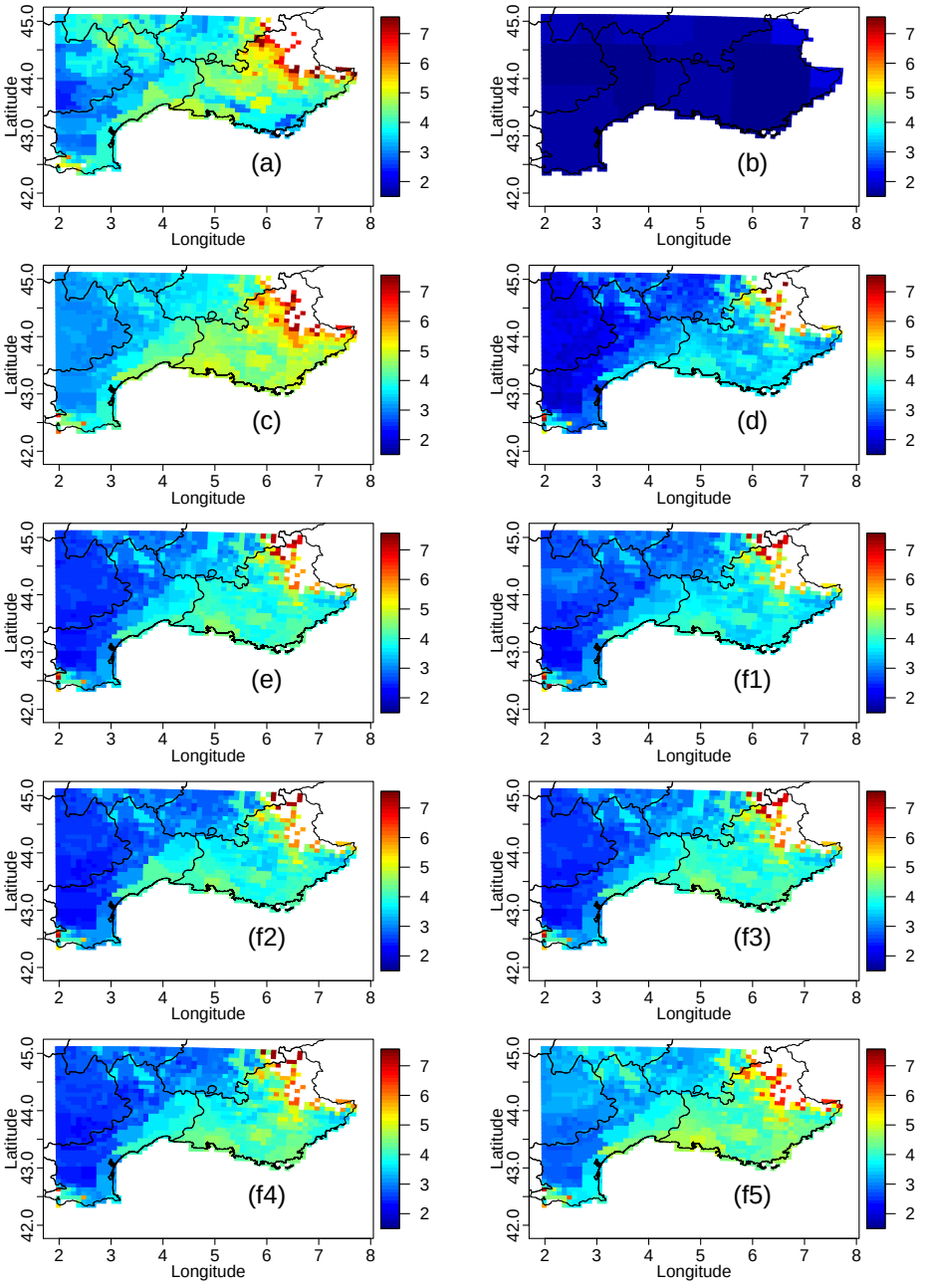


**Figure 13.** Same as Fig. 12 but for mean dry spell lengths. The upper bound has been constrained for visualization purposes.

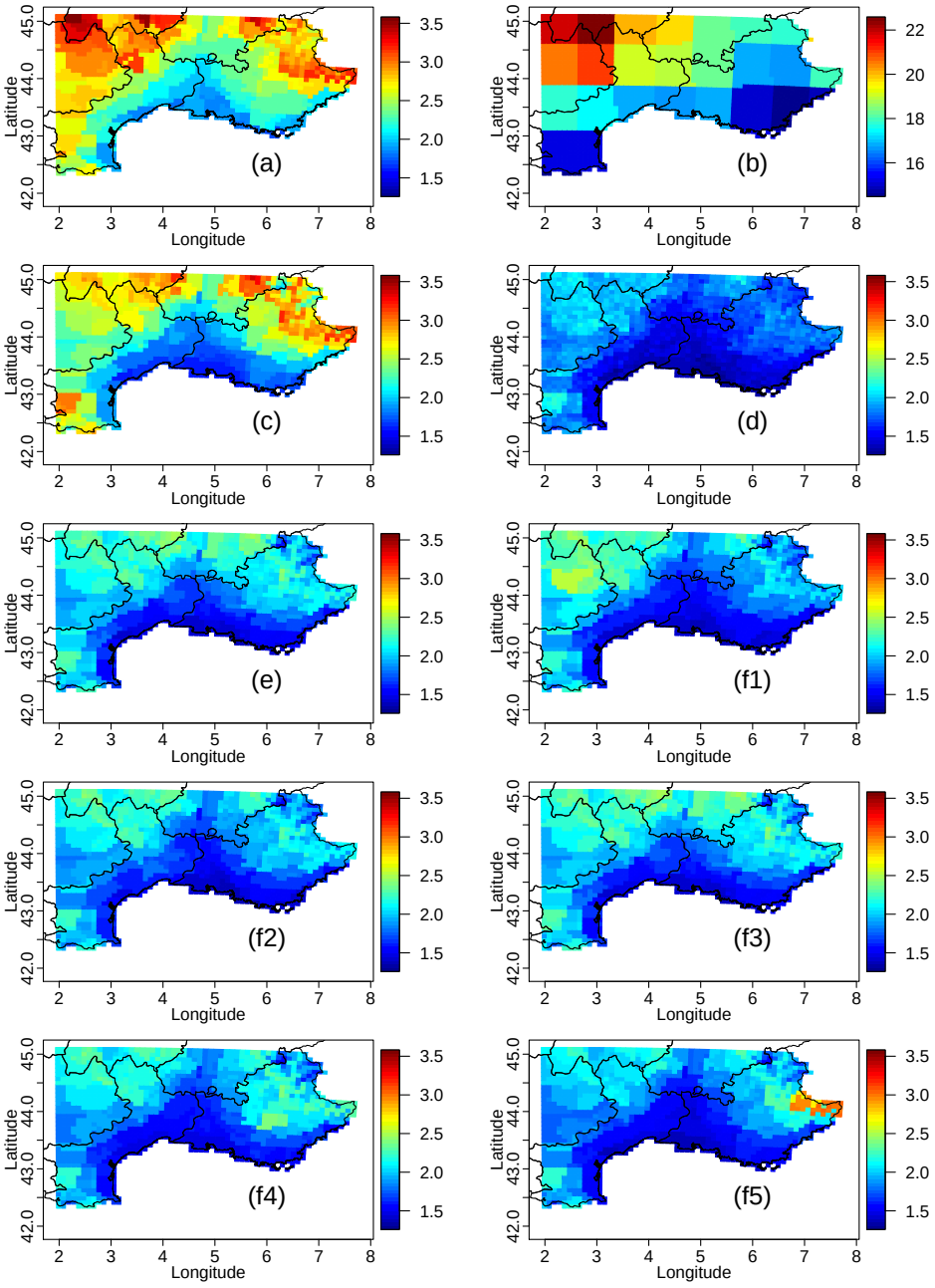


**Figure 14.** Maps of the mean wet spell lengths in summer for (a) SAFRAN; (b) ERAI; (c) 1d-BC; (d) 2d-$R^2D^2$; (e) 1506d-$R^2D^2$ (PR); (f1-5) 3012d-$R^2D^2$ with 5 different reference temperature locations. Note that the ERA-I sub-figure (b) has a range different from the others for visualization purposes.

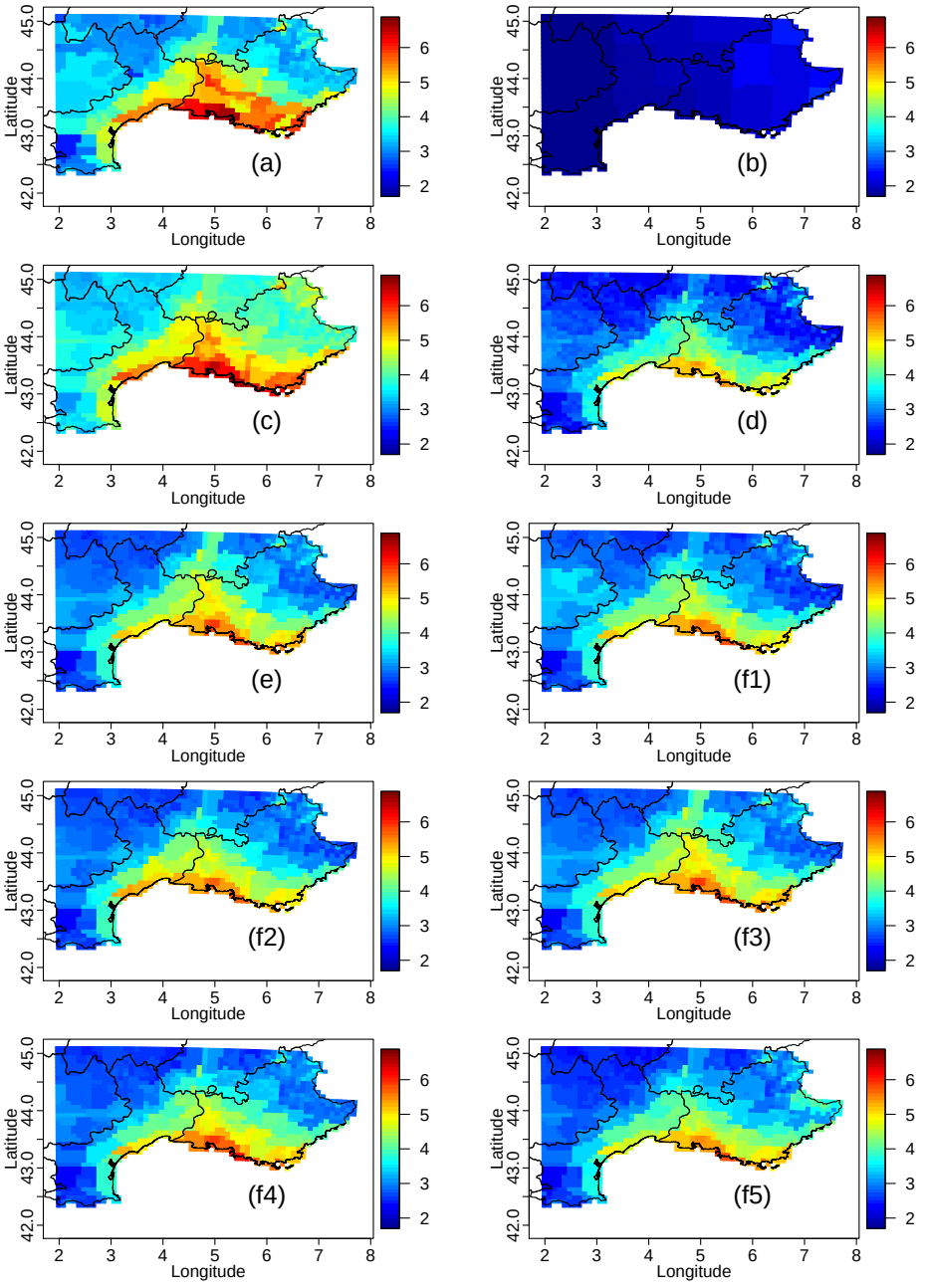


**Figure 15.** Same as Fig. 14 but for mean dry spell lengths. The upper bound has been constrained for visualization purposes.

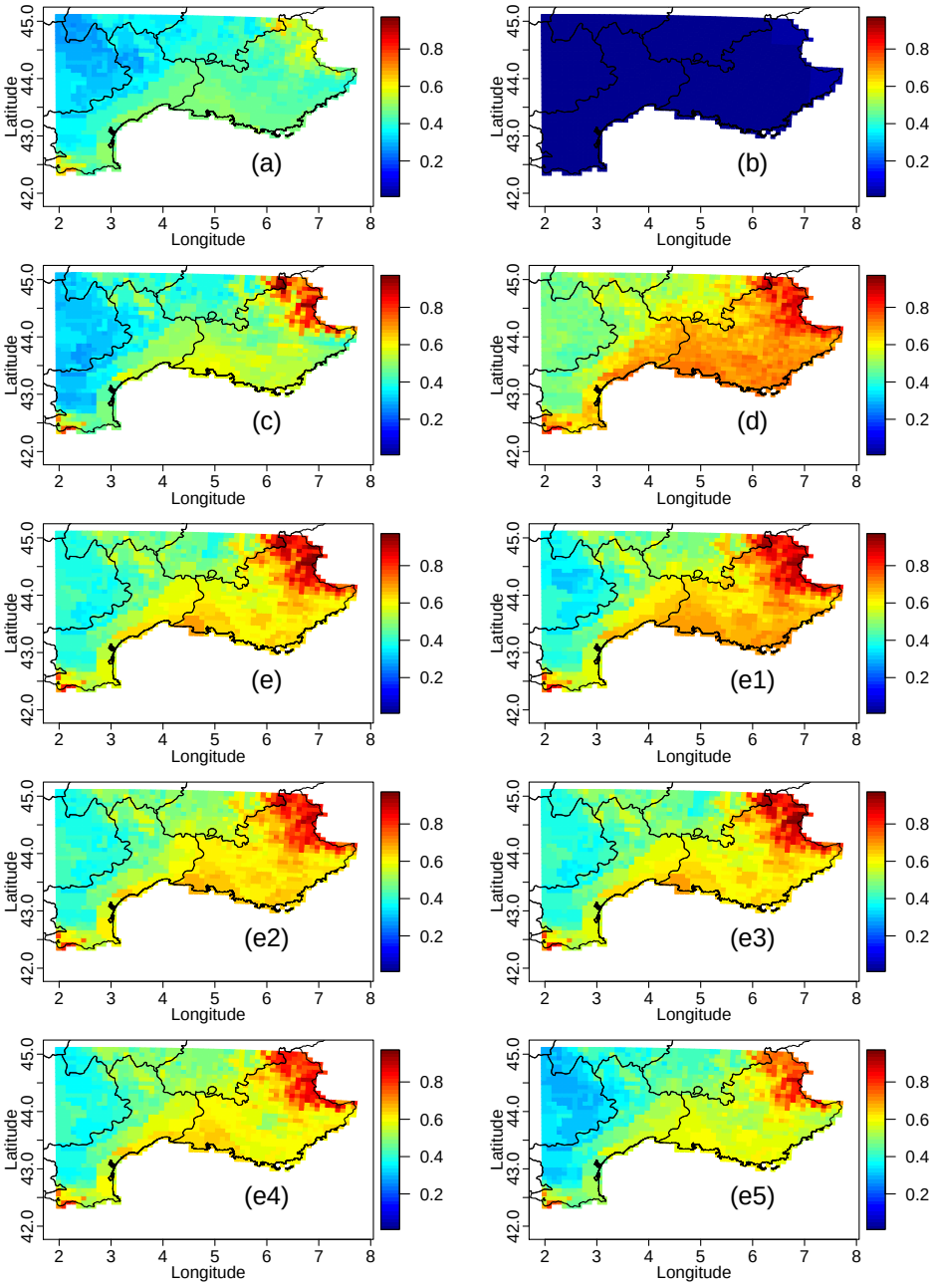


**Figure 16.** Winter probabilities of a dry day given that the previous day is wet for (a) SAFRAN; (b) ERAI; (c) 1d-BC; (d) 2d-$R^2D^2$; (e) 1506d-$R^2D^2$ (PR); (f1-5) 3012d-$R^2D^2$ with 5 different reference temperature locations.

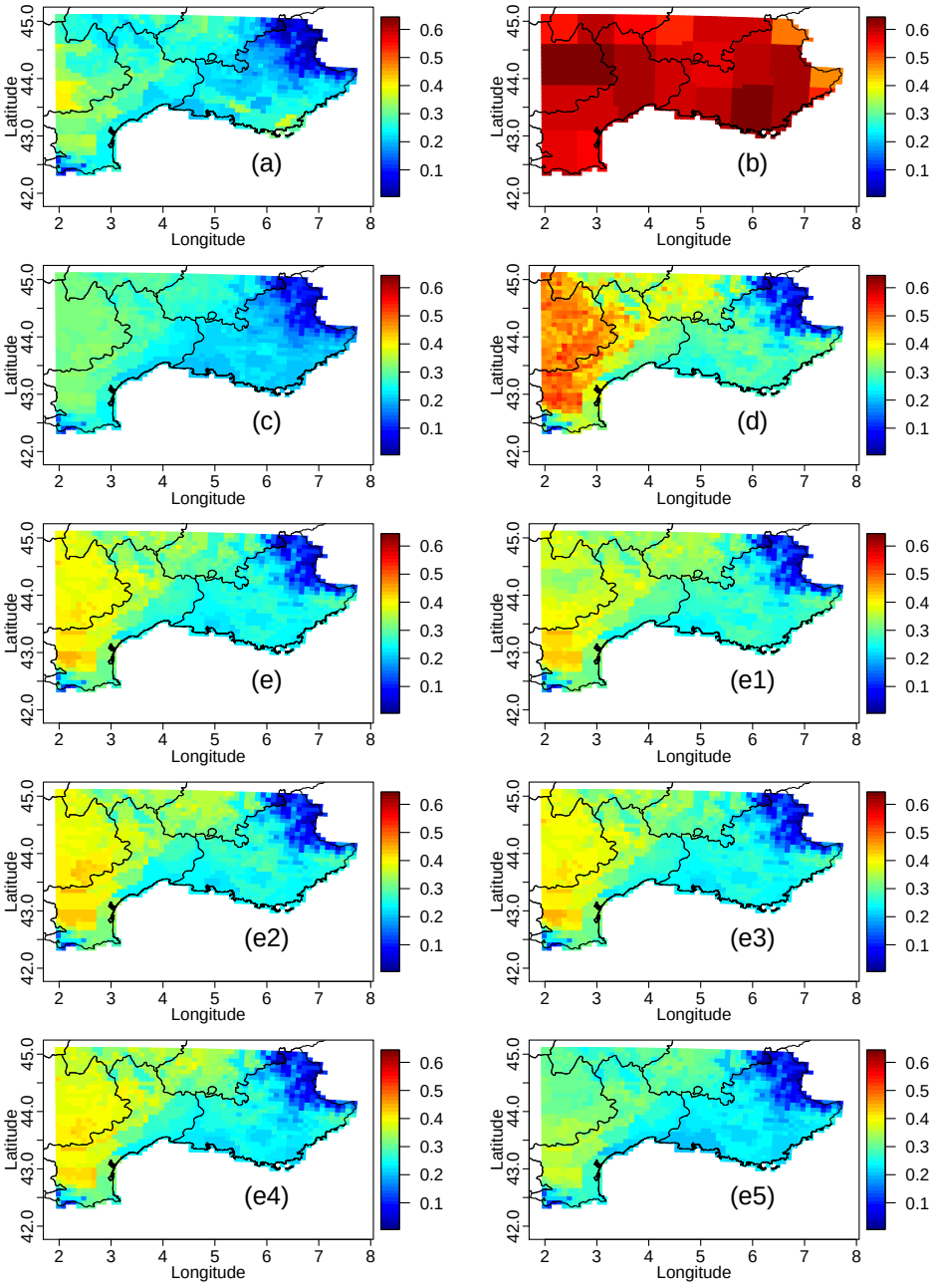


**Figure 17.** Winter probabilities of a wet day given that the previous day is dry for (a) SAFRAN; (b) ERAI; (c) 1d-BC; (d) 2d-$R^2D^2$; (e) 1506d-$R^2D^2$ (PR); (f1-5) 3012d-$R^2D^2$ with 5 different reference temperature locations.

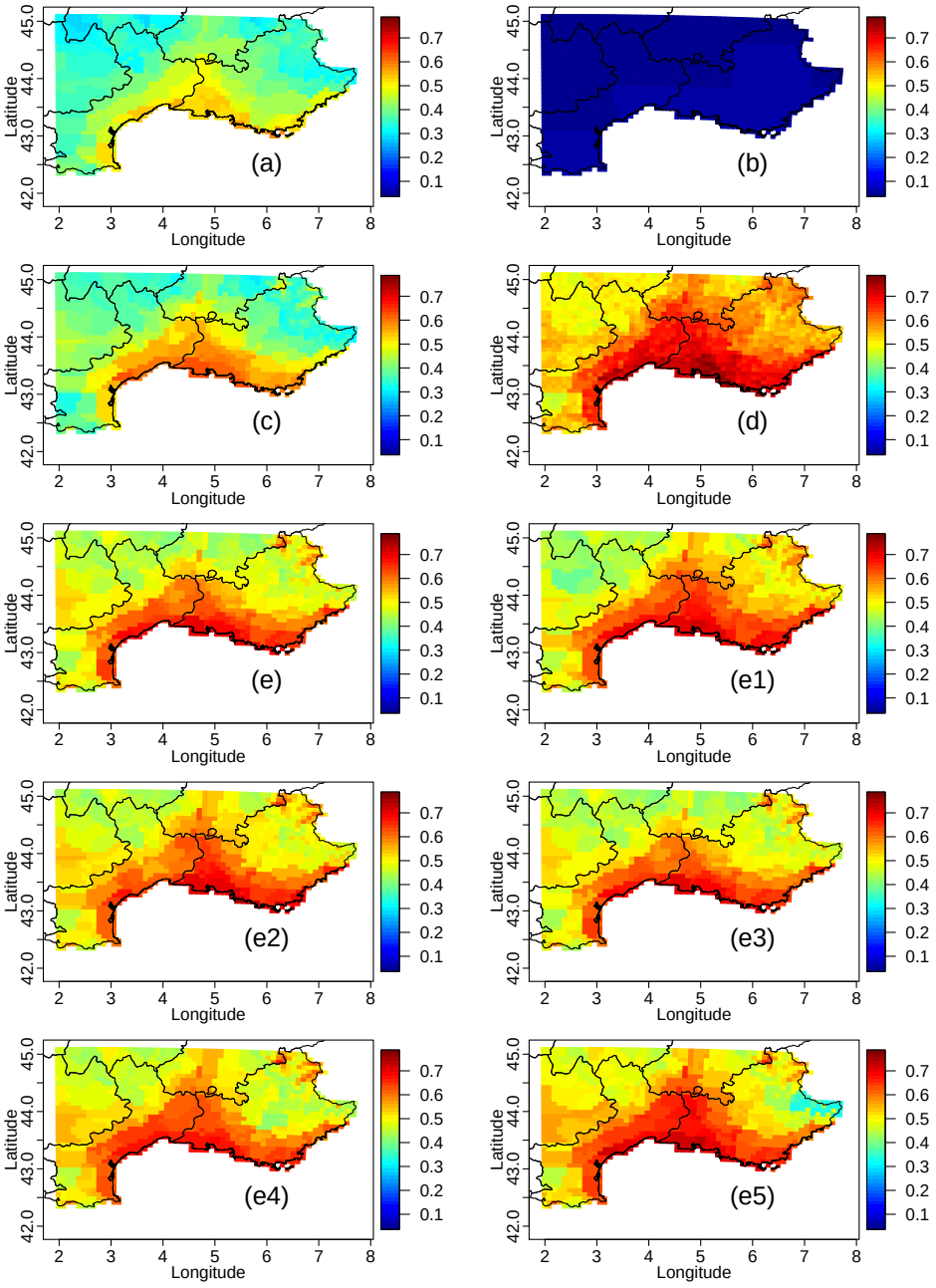


**Figure 18.** Summer probabilities of a dry day given that the previous day is wet for (a) SAFRAN; (b) ERAI; (c) 1d-BC; (d) 2d-$R^2D^2$; (e) 1506d-$R^2D^2$ (PR); (f1-5) 3012d-$R^2D^2$ with 5 different reference temperature locations.

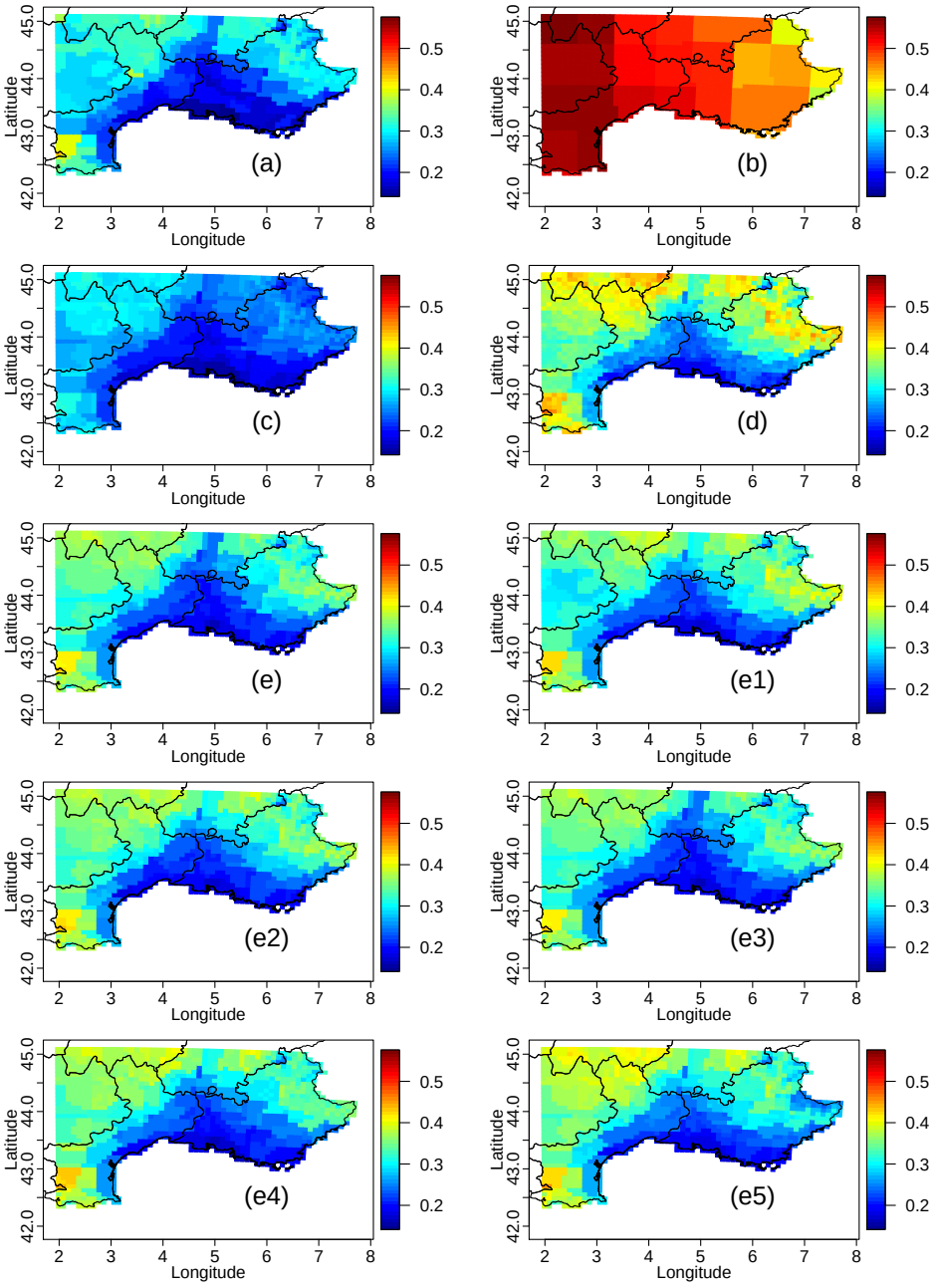


**Figure 19.** Summer probabilities of a wet day given that the previous day is dry for (a) SAFRAN; (b) ERAI; (c) 1d-BC; (d) 2d-$R^2D^2$; (e) 1506d-$R^2D^2$ (PR); (f1-5) 3012d-$R^2D^2$ with 5 different reference temperature locations.

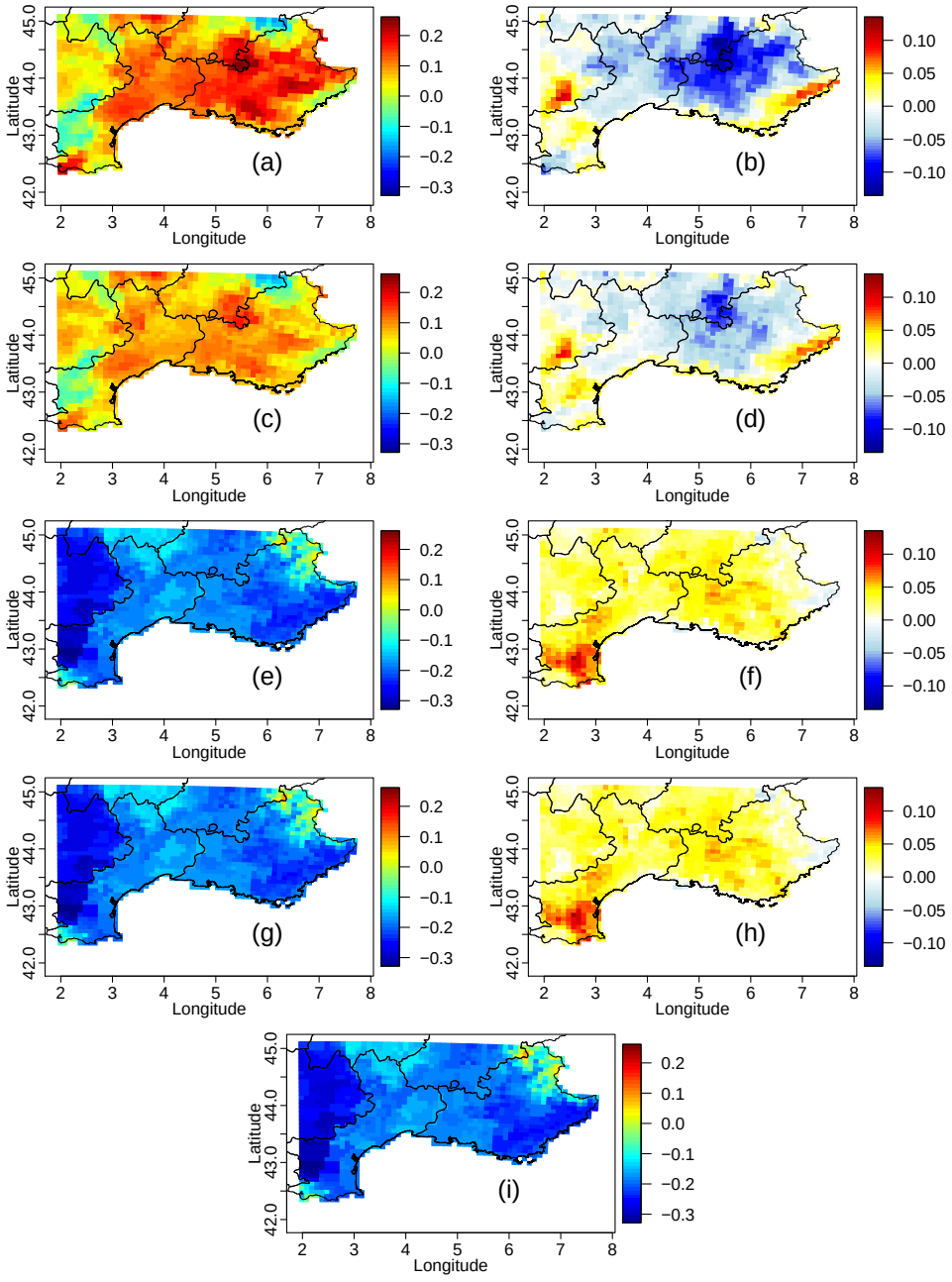


**Figure 20.** (left column) Intervariable Pearson correlations between T2 and PR in Summer for each grid cell and (right column) changes in intervariable Pearson correlations from the historical period to the 2071-2100 period; (a-b) for the WRF RCM; (c-d) for its 1d-bias correction with CDF-t; (e-f) for its 2d-$R^2D^2$ correction; (g-h) for its 3012d-$R^2D^2$ correction. Panel (i) corresponds to the correlations between T2 and PR for the SAFRAN reference data over the historical period

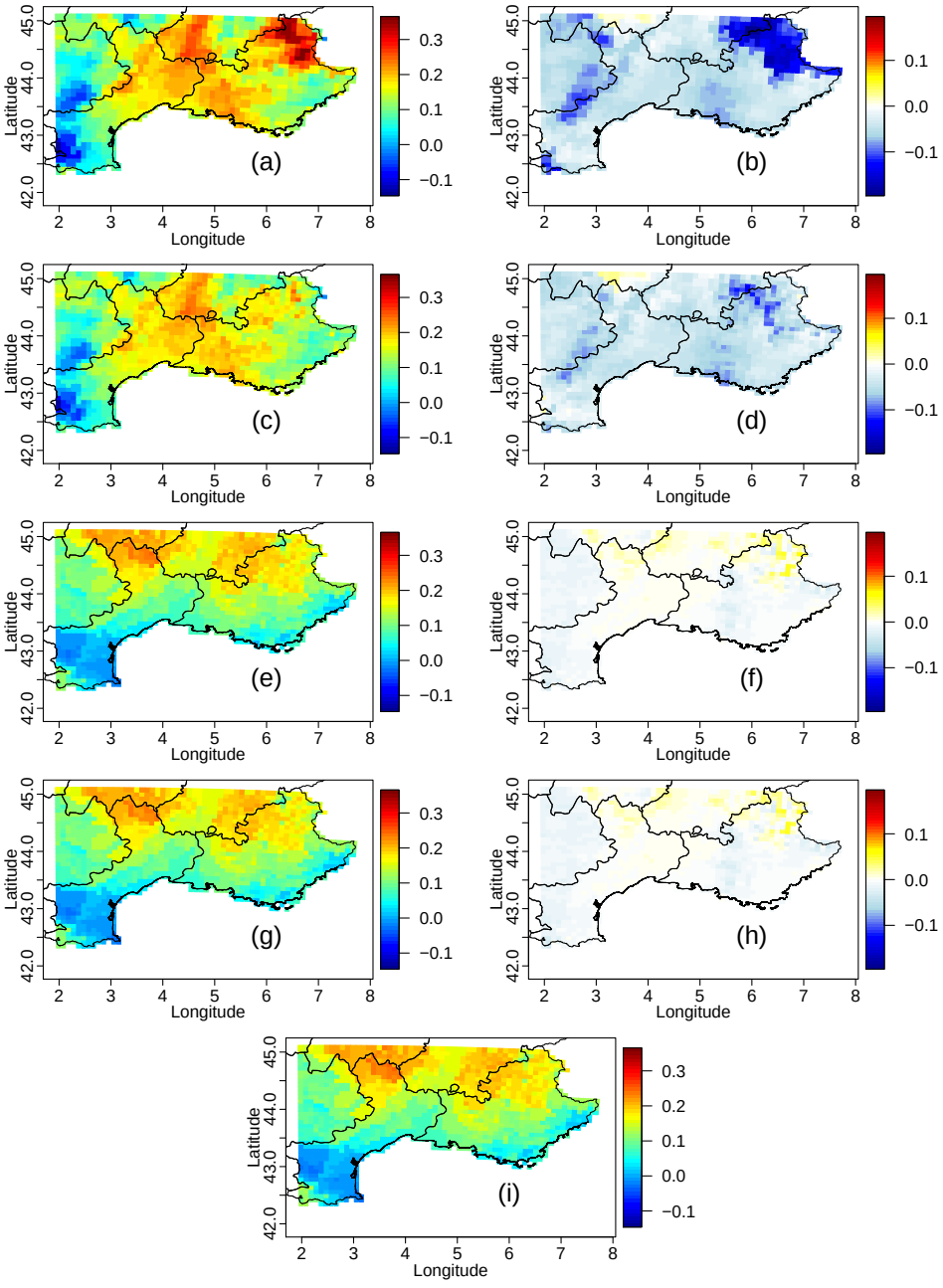


**Figure 21.** Same as Fig. 20 but from the RCA4 RCM in Winter.

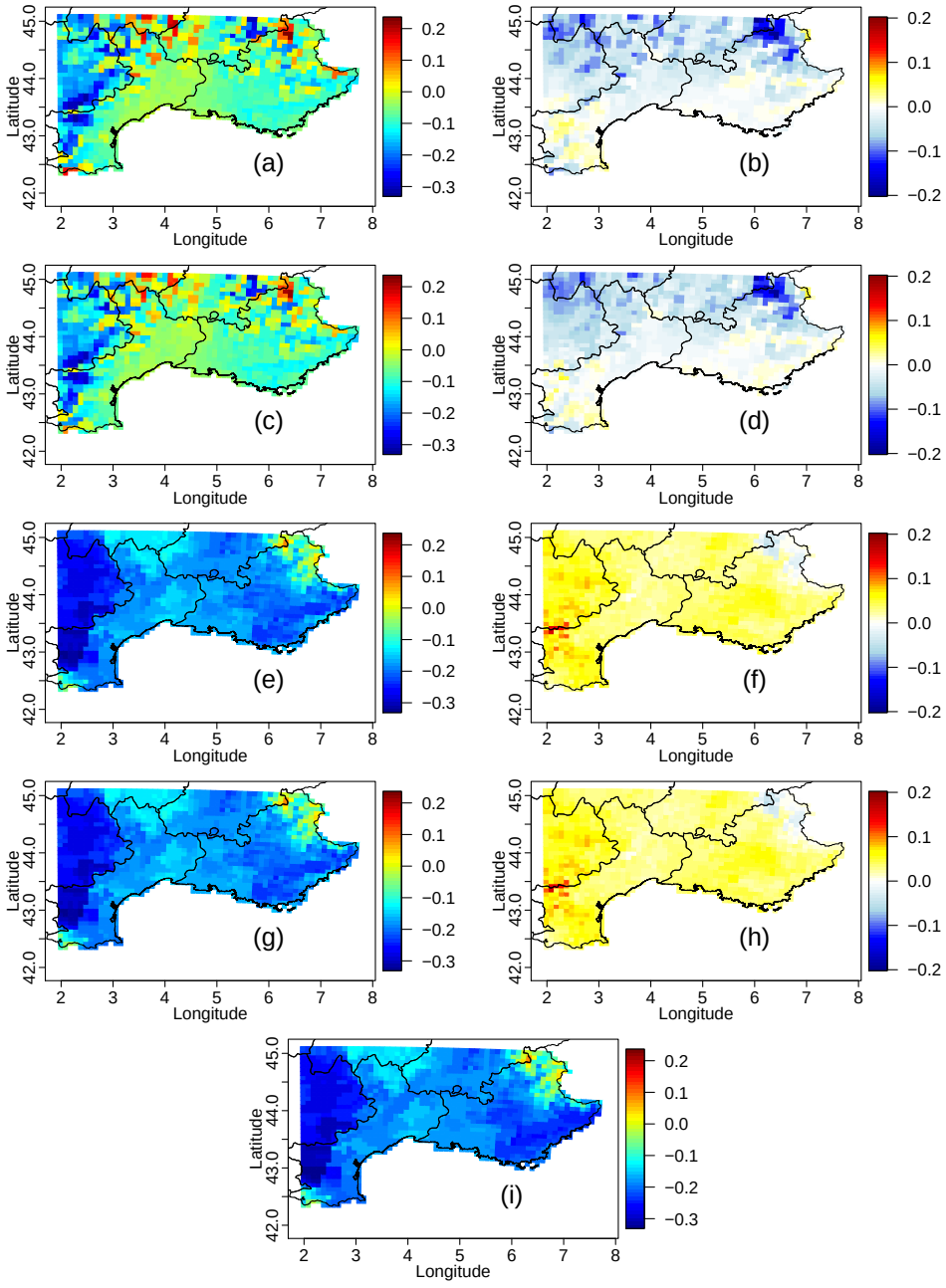


**Figure 22.** Same as Fig. 20 but from the RCA4 RCM in Summer.

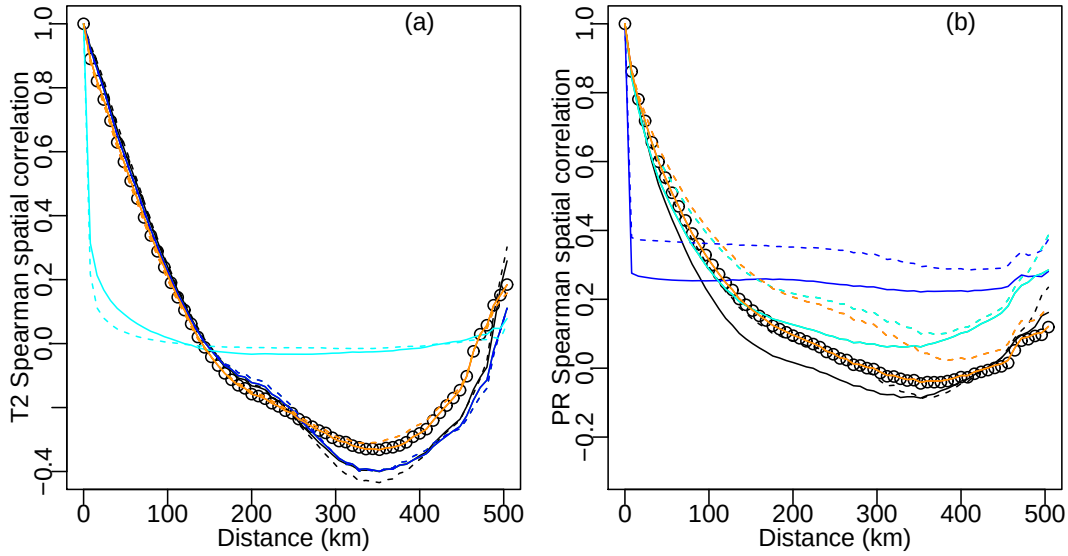


**Figure 23.** Spatial correlograms of temperature (a) and precipitation (b) in summer computed from daily areal mean-removed data. Correlations from SAFRAN are in circles; those from the WRF RCM are in black lines; 1d-BC in green; 2d-$R^2D^2$ driven by temperature in blue; 2d-$R^2D^2$ driven by precipitation in cyan; 3012d-$R^2D^2$ driven by temperature at a given location in red; 3012d-$R^2D^2$ driven by precipitation at the same location in orange. Solid lines indicate results for the historical period, dashed lines for the 2071-2100 period. Note that for temperature results (a), green and blue lines are superimposed. For precipitation (b), green and cyan are superimposed. Red and orange lines are always superimposed for both (a) and (b).

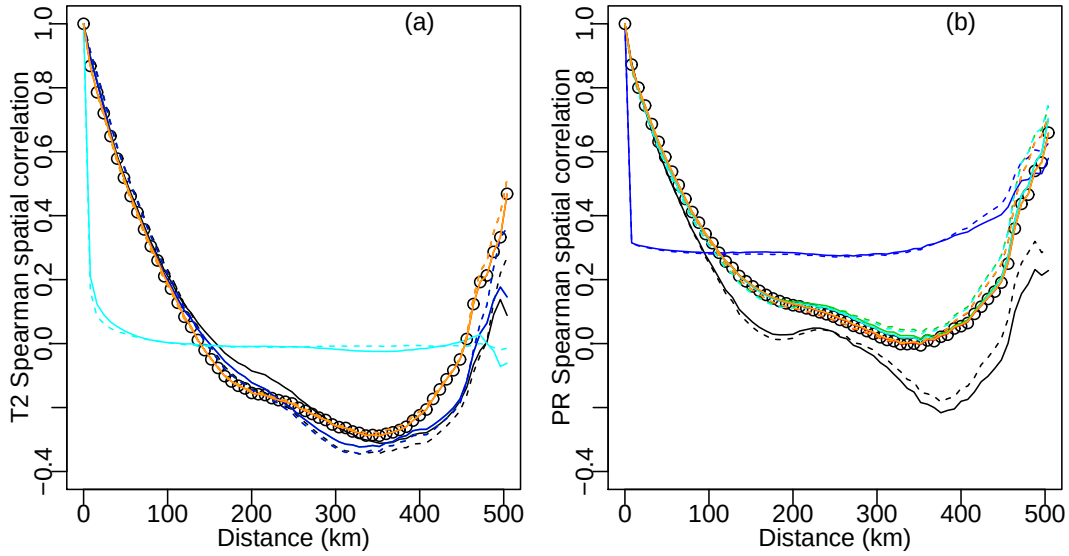


**Figure 24.** Same as Figure 23 but for RCA4 in winter.

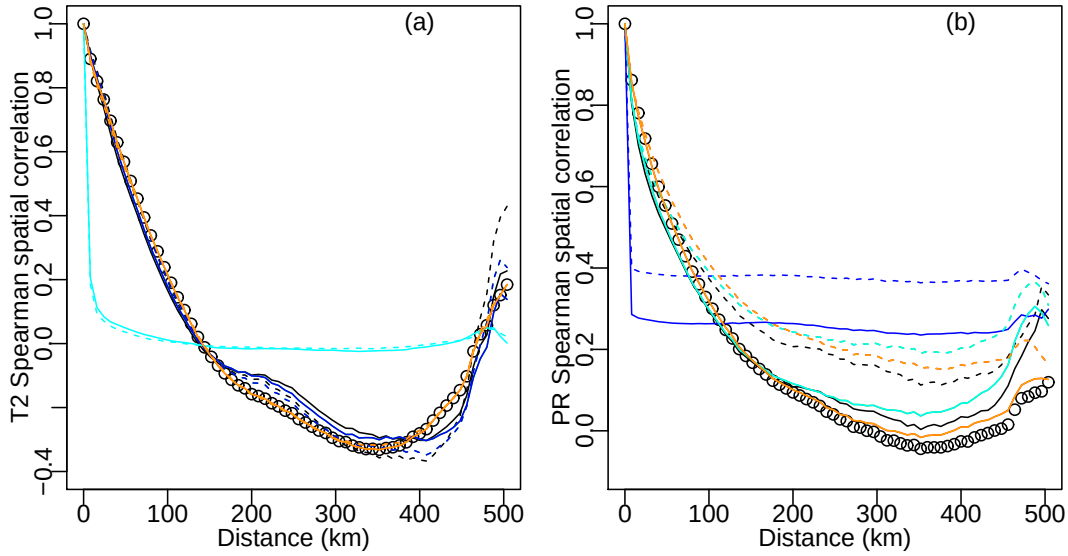


**Figure 25.** Same as Figure 23 but for RCA4 in summer.